Applied Mathematics Letters 86 (2018) 291–297

Contents lists available at ScienceDirect

Applied Mathematics Letters

www.elsevier.com/locate/aml

Continuation methods for time-periodic travelling-wave solutions to evolution equations

T.-S. Lin[a], D. Tseluiko[b], M.G. Blyth[c,*], S. Kalliadasis[d]

[a] *Department of Applied Mathematics, National Chiao Tung University, Hsinchu 30010, Taiwan*
[b] *Department of Mathematical Sciences, Loughborough University, Loughborough, LE11 3TU, UK*
[c] *School of Mathematics, University of East Anglia, Norwich, NR4 7TJ, UK*
[d] *Department of Chemical Engineering, Imperial College London, London, SW7 2AZ, UK*

ARTICLE INFO

Article history:
Received 23 February 2018
Received in revised form 28 June 2018
Accepted 28 June 2018
Available online 7 July 2018

Keywords:
Numerical continuation
Evolution equation
Long-wave model

ABSTRACT

A numerical continuation method is developed to follow time-periodic travelling-wave solutions of both local and non-local evolution partial differential equations (PDEs). It is found that the equation for the speed of the moving coordinate can be derived naturally from the governing equations together with a condition that breaks the translational symmetry. The derived system of equations allows one to follow the branch of travelling-wave solutions as well as solutions that are time-periodic in a frame of reference travelling at a constant speed. Finally, we show as an example the bifurcation and stability analysis of single and double-pulse waves in long-wave models of electrified falling films.

1. Introduction

We present a novel numerical continuation method which can be used to explore solutions of evolution equations with translational invariance. The method can be used to construct detailed bifurcation diagrams that include travelling wave solutions and their bound states as well as pulsating travelling wave solutions. Travelling waves are stationary in a frame travelling at constant speed. Pulsating travelling waves are time-periodic in a frame of reference travelling at constant speed. An appropriate condition must be imposed to break the translational invariance. Normally there is also another symmetry associated with the fact that a new solution can be created from a given travelling wave solution by altering its volume. By treating the evolution equation in a moving frame as an infinite-dimensional dynamical system, steady states and time-periodic states can be obtained as fixed points and periodic orbits of this dynamical system. The speed of the moving frame is one of the unknowns and it can be eliminated by using the translational symmetry-breaking condition. Consequently we can exploit existing continuation methods for infinite-dimensional dynamical systems to explore the bifurcation structure for the evolution equation. A similar technique was developed

* Corresponding author.
E-mail address: m.blyth@uea.ac.uk (M.G. Blyth).

https://doi.org/10.1016/j.aml.2018.06.034
0893-9659/

by Lin et al. [1] to study the motion of a liquid film on the outside of a horizontal rotating cylinder; in this case there is no translational symmetry due to gravity. In the present work we apply our new continuation method to the particular case of a thin liquid film flowing down an inclined plane in the presence of an electric field.

The description of the method is presented in Section 2 and in Section 3 we present our results including detailed bifurcation diagrams and time-periodic solutions. Finally in Section 4 we summarise our findings.

2. Numerical continuation of solutions of evolution equations

Consider the general one-dimensional evolution equation

$$\partial_t h = \partial_x \left(F[h] \right), \tag{1}$$

where F is a nonlinear differential or pseudo-differential operator (see for example [2]), $h = h(x, t)$, x and t are spatial and time variables, respectively. We assume that this equation possesses translational symmetry, namely, we assume that for a translation operator T_y (i.e. an operator such that $T_y[f](x) = f(x - y)$ for any function f), we have $T_y \circ F = F \circ T_y$ for any $y \in \mathbb{R}$. We will consider this equation on a periodic domain $x \in [-L, L]$. Introducing into (1) a moving coordinate via the mapping $x \mapsto x - s(t)$, we have

$$\partial_t h = \dot{s}\partial_x h + \partial_x \left(F[h] \right), \tag{2}$$

where the dot over s is used to denote the time derivative. We note that $\dot{s}$ corresponds to the speed of the moving frame. We consider the general case where $\dot{s} = \dot{s}(t)$, so that the speed is a function of time.

To perform continuation in the parameter space, we need two additional conditions. One condition is needed to break the translational symmetry. We choose the following,

$$\int_{-L}^{L} h \sin(nqx) \mathrm{d}x = 0, \tag{3}$$

where $q = \pi/L$ and n is a chosen integer. A second condition is needed to break the volume symmetry. This symmetry stems from the fact that, given a travelling-wave solution, by slightly changing the volume, $\int_{-L}^{L} h \, dx$, we obtain a new solution. To break this volume symmetry, we can, for example, choose to fix the average thickness:

$$\frac{1}{2L} \int_{-L}^{L} h \, \mathrm{d}x = \alpha, \tag{4}$$

where α is a constant. Other possibilities will be considered below.

Next, we rewrite (2) as an infinite-dimensional system of ordinary differential equations for the Fourier coefficients of h. Truncating this system at a sufficiently high wavenumber to retain an accurate representation for h, we obtain

$$h(x, t) = c_0(t) + \sum_{k=1}^{N} [c_{2k-1}(t) \cos(kqx) + c_{2k}(t) \sin(kqx)], \tag{5}$$

where the c_i's are the Fourier coefficients of h and N is a sufficiently large integer. Conditions (3) and (4) respectively imply that

$$c_{2n} = 0, \qquad c_0 = \alpha. \tag{6}$$

The system of ordinary differential equations for the c_i's has the form

$$\dot{c_i} = \mathcal{N}_i(c_0, \ldots, c_{2N}), \quad i = 1, \ldots, 2n - 1, 2n + 1, \ldots, 2N, \tag{7}$$

where the $\mathcal{N}_i$'s are nonlinear functions of all the Fourier coefficients. In our numerical calculations, we compute the $\mathcal{N}_i$'s for given c_i's by first using the inverse fast Fourier transform to compute h and the

right-hand side of (2), and applying the fast Fourier transform to the right-hand side of (2) to obtain $\mathcal{N}_i(c_0, \ldots, c_{2N})$.

Multiplying (2) by $\sin(nqx)$ and integrating over the domain, we find that the speed, $\dot{s}$, should satisfy

$$\dot{s} = \frac{-\int_{-L}^{L} \partial_x \left(F[h]\right) \sin(nqx)\, \mathrm{d}x}{\int_{-L}^{L} \partial_x h \sin(nqx)\, \mathrm{d}x}. \tag{8}$$

Travelling-wave solutions of (1) correspond to steady-state solutions of (7), where the speed is given by (8) and is a constant. By performing continuation with respect to a parameter that may be present in the equation or with respect to the domain size, we can obtain branches of travelling-wave solutions. We implement this by utilising the continuation and bifurcation software AUTO07p [3,4] together with the FFTW3 package [5] for computing fast Fourier transforms. (We note that a similar Auto07p+FFTW coupling was developed to study, for example, spiral waves [6] and the coarsening of aggregating particles [7], and a more detailed note on the history of such a coupling can be found in [1].) Nonlinearities are de-aliased using the zero-padding technique [8]. In addition to following travelling-wave branches, our method allows us to continue onto branches of time-periodic solutions (within the travelling frame). Such branches are expected to emerge via Hopf bifurcations on the travelling wave branches. As far as time-periodic solutions are concerned, the computed wave speed $\dot{s}$ is not constant, but is a time-periodic function. However, we can view the solution as being time-periodic in a frame of reference moving at a constant speed equal to the average of $\dot{s}$ over one time period.

For a travelling-wave solution, taking the limit $L \to \infty$ yields a solitary pulse on the infinite domain that approaches the constant α as $x \to \pm\infty$. However, for the computation of such solitary pulses it may be more convenient to use a different set of conditions instead of (3) and (4). For example, to break the translational symmetry, one can impose the condition $\partial_x h = 0$ at $x = 0$ instead of (3), which in the Fourier space takes the form $\sum_{k=1}^{N} k c_{2k} = 0$, and to break the volume symmetry, we can impose the condition $h = \alpha$ at $x = L$ instead of (4), which in the Fourier space takes the form $c_0 + \sum_{k=1}^{N} (-1)^k c_{2k-1} = \alpha$.

Alternatively, by integrating the steady version of Eq. (2), we find that a steady solution satisfies

$$\dot{s}h + F[h] = C_1, \tag{9}$$

where C_1 is a constant of integration. By assuming that $h \to \alpha$ at $x \to \pm\infty$, we obtain $C_1 = \dot{s}\alpha + F[\alpha]$, which may be considered as a condition breaking the volume symmetry. Instead of solving (2), we can now solve (9). Furthermore, the pulse speed can be eliminated by integrating (9) over the domain, which gives

$$\dot{s} = -\frac{\int_{-L}^{L} (F[h] - F[\alpha])\mathrm{d}x}{\int_{-L}^{L} (h - \alpha)\, \mathrm{d}x}, \tag{10}$$

assuming that $\int_{-L}^{L} (h - \alpha)\mathrm{d}x \neq 0$.

It is worth mentioning at this point the freely-available Matlab software package `pde2path` [9] to perform continuation to follow bifurcation branches. The present methodology was communicated to the developers of `pde2path` already back in 2015, while recently `pde2path` has been extended with a facility to follow pulsating travelling-wave solution branches (see the tutorials in [10,11]).

3. Case study: Electrified flow down an inclined plane

We now apply the method introduced in the previous section to explore the bifurcation structure of solutions of a non-local thin liquid film model,

$$h_t + \left[h^3 \left(\frac{2\sin\beta}{3} - \frac{2\cos\beta}{3} h_x + \frac{1}{3Bo} h_{xxx} + \frac{2}{3} We\, \mathcal{H}[h_{xx}]\right)\right]_x = 0. \tag{11}$$

This model describes the evolution of the free surface of an electrified liquid film flowing down an inclined plane wall [12]. Here, $h(x,t)$ denotes the film thickness at position x at time t, the plane wall is inclined at angle β to the horizontal, and Bo and We are the Bond and electric Weber number, respectively (see [12]). These measure, respectively, the relative effects of gravity to surface tension, and of the electric field to gravity. The Hilbert transform $\mathcal{H}$ is defined by $\mathcal{H} = \frac{1}{\pi}\text{p.v.}\int_{-\infty}^{\infty} f(\tilde{x})/(x-\tilde{x})\mathrm{d}\tilde{x}$, where p.v. denotes the principal value. Note that the Hilbert transform operator has the symbol $-\mathrm{i}\,\mathrm{sgn}(k)$ in the Fourier space.

For certain parameter values, the long-time evolution of solutions to (11) is described by a superposition of weakly interacting single-hump pulses, each of which resembles a single-hump solitary pulse. The pulses can attract and repel each other and can form bound states, that is two or more pulses travelling at the same speed as a group. This is an example of a self-organisation process [13]. Such states are therefore of great interest and we herein exploit the current method to study them.

The single-hump solitary pulse solutions can be found by solving (11) using numerical continuation techniques. We consider solutions on a periodic domain, $x \in [-L, L]$, and start the continuation using a small nearly sinusoidal perturbation from the cut-off wavelength for linear instability $L_c = 2\pi/\kappa_c$ where

$$\kappa_c = Bo\,We + \sqrt{Bo^2\,We^2 - 2Bo\cos\beta} \tag{12}$$

(see [12]). We continue on this branch of single-pulse travelling wave solutions by increasing the domain size L. The computations in this section were performed using the conditions (3), (4) to break the translational and volume symmetry, respectively, and use the formulation (8) for the pulse speed. We also fix $\alpha = 1$ and the parameters $\beta = 0.95\pi$, $Bo = 0.005$ and $We = 2.25$ for which values we expect the model equation (11) to be valid.

3.1. Calculation of bound states by numerical continuation

To look for two-pulse bound states, we again start the continuation using a small-amplitude nearly sinusoidal solution of nearly cut-off wavenumber, $k \approx \kappa_c$, on the domain $[-L, L]$, with $L \equiv 2\pi/k$. With this choice we note that two periods of the small amplitude wave are included in the computational domain, i.e. we start with a two-mode solution. As most of the two-pulse bound states have nearly identical L^2-norm, we characterise solutions using the semi-norm $\chi_n(h^*) \equiv |\int_{-L}^{L} h^*(x)\cos(\pi n x/L)\,\mathrm{d}x|$, for integer n. An example is shown in Fig. 1(a). The starting point for the continuation is denoted by a filled circle at $L = 2\pi/\kappa_c \approx 56.47$ and the corresponding branch is shown by the solid line. As the branch is followed, eventually when L is sufficiently large the profile develops into one with two single-pulse solutions 'glued' together with separation distance equal to L. We note, however, that this is not a bound state but rather a spatially periodic solution with effective period L.

The filled diamonds along the branch represent bifurcation points to side branches shown by dashed lines in the figure. We identified 12 such bifurcation points. By following the first bifurcation branch which emerges from the lowest branch point, we actually obtain a negative solitary-pulse solution at large L. The pulse profile is shown in Fig. 1(b) at $L = 400$, corresponding to the empty circle symbol in panel a. We note that the far-field level is almost equal to unity.

The next seven bifurcation points and corresponding side branches lead to two-pulse bound state solutions at large L. The profiles corresponding to the second and the eighth branches are depicted in Fig. 1(c). The profile with a solid line corresponds to the top square symbol in panel a the branch that bifurcates from the main branch at smallest value of L (among the seven identified two-pulse bound state branches), and consequently the two-pulse bound state solution on this branch has the smallest separation distance. The profile with a dashed line corresponds to the bottom square symbol in panel a and is on the branch that bifurcates from the main branch at the largest value of L (among the two-pulse bound-state branches), and is the two-pulse bound state with the largest separation distance.

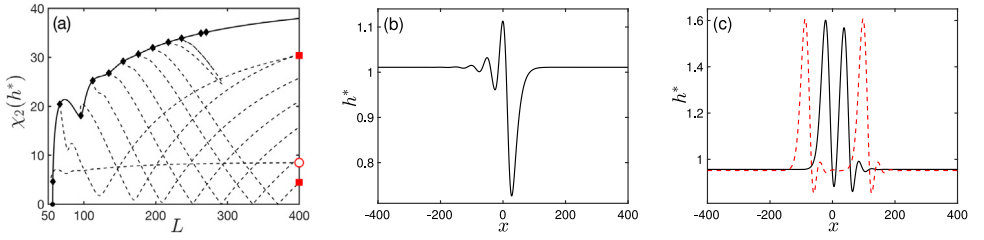

Fig. 1. (Colour online) (a) Bifurcation diagram of travelling-wave solutions to (11) with $\beta = 0.95\pi$, $Bo = 0.005$ and $We = 2.25$. The solid line is the main branch that indicates the two-mode travelling wave solution with equal separation distance. The diamonds indicate branch points (BP) which correspond to pitchfork bifurcations. All the dash lines are branches that bifurcate from the BPs in the main branch. (b) The negative-pulse solution on the first side branch in (a). (c) Two-pulse bound states on the side branches emerging from the second (black-solid line) and eighth (red-dashed line) branch points in (a), reading from left to right.

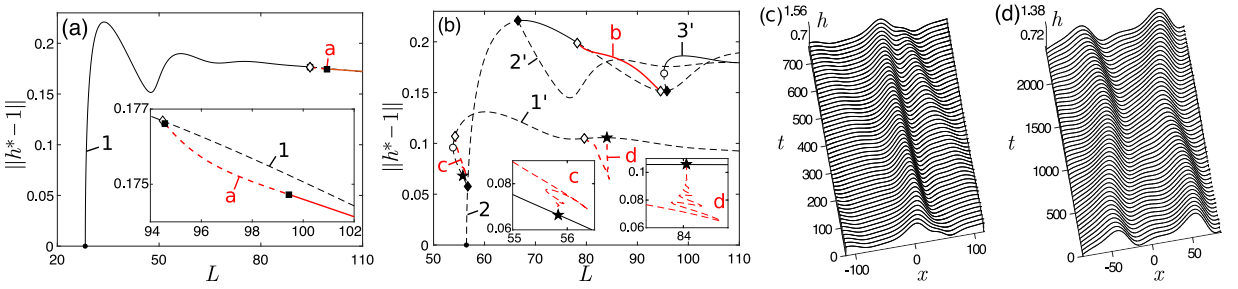

Fig. 2. (Colour online) (a, b) Bifurcation structure of solutions for the long-wave model (11) with $\beta = 0.95\pi$, $Bo = 0.005$ and $We = 2.25$. (c) The time-periodic solution on branch a at $L = 116.1$. (d) The time-periodic solution on branch b at $L = 86.1$. See the supplementary material for movies of the time-periodic solutions ('movie1.avi' and 'movie2.avi' respectively for panels c and d). The symbols and line styles used in the panels are explained in the text.

There are four more branch points at $L \approx 217.4$, 235.9, 262.8 and 270.4. Side branches connect the first and second pairs of these to each other (the latter branch connection is barely visible in panel a) and so do not extend to large L and do not produce bound-state solutions. We conclude that in this case there are only 7 two-pulse bound states. This is consistent with the weak interaction theory of [12] in that in the present case with a non-local effect of the electric field there are only a finite number of two-pulse bound states.

3.2. Bifurcation diagrams: extension to time-periodic solutions

The solutions that we have discussed so far are positive single-pulse, positive multi-pulse and negative pulse solutions. All of these are travelling waves that are stationary in the moving frame. There is a vast literature on the computation of bifurcation diagrams of such solutions, both for weakly nonlinear models such as the Kuramoto–Sivashinsky equation (e.g. [14]) and fully nonlinear models similar to (11) (e.g. [15]). However, there exist other solutions such as pulsating waves that are time-periodic in a frame of reference travelling at a constant speed which is unknown in advance. Using continuation techniques developed in Section 2, we are able to track branches of travelling-wave solutions as well as time-periodic solutions, so that we can construct more detailed bifurcation diagrams of a given system and obtain a better understanding of the solution space.

In Fig. 2, we present bifurcation diagrams showing branches of single-pulse solutions (panel a) and two-pulse solutions (panel b) as well as time-periodic solutions. The stability of each of the branches was determined by calculating the eigenvalues and Floquet multipliers of the travelling-wave and time-periodic solutions (see, for example, [16] for details of how to do this). Stable and unstable parts of the branches

are shown with solid and dashed lines, respectively. Numbers are used to label primary branches of steady travelling-wave solutions and letters are used to label branches of time-periodic solutions appearing from Hopf bifurcations (HBs) indicated by empty diamonds. Numbers with dashes are used to denote side branches of steady travelling-wave solutions appearing from pitchfork bifurcations (PBs) (strictly speaking, pitchfork bifurcations of revolution due to the translation symmetry) indicated by filled diamonds. Saddle–node bifurcations (SNs) are indicated by empty circles.

Branches 1 and 2 of single- and double-pulse solutions, respectively, emerge from the filled circles at the cut-off wavelengths $L \approx 28.23$ and 56.47. (Of course, branches of three-pulse solutions, and so on, bifurcate from higher values of L but these are not shown.) The branch of single-pulse solutions is stable from the bifurcation point at $L \approx 28.2$ up to the appearance of the HB point at $L \approx 94.5$. The latter bifurcation is supercritical and the branch a which emerges from it is therefore stable at least in the region close to the bifurcation point. In fact we find that a period-doubling bifurcation (shown with a filled square, seen more clearly in the inset) occurs on the time-periodic branch a after only a short distance, where the stability of solutions on branch a is lost. Stability is recovered after another period-doubling bifurcation (also shown with a filled square, and seen more clearly in the inset) at $L \approx 99.4$. We are able to follow the branches which emerge from these period-doubling bifurcations using the current method. In fact a continuous side branch (not shown) is found to connect the two, and further period-doubling bifurcations are found to occur along this side branch. The stable time-periodic solution on branch a at $L = 116.1$ is shown in panel c of the figure. One period of evolution of 743.7 dimensionless time units is shown in a frame of reference moving at speed $c = 0.4$. We observe a single pulse moving over a non-uniform background of smaller amplitude and slower waves.

The only stable parts of branch 2 in the range shown are between the PB at $L \approx 66.5$ and the HB at $L \approx 78.3$, and between the HB at $L \approx 94.5$ and the PB at $L \approx 95.7$. It should be noted the two HBs shown on branch 2 are connected by branch b of stable time-periodic solutions. The time-periodic solution on this branch at $L = 86.1$ is shown in panel d of the figure in a frame of reference moving at speed $c = 0.3$. One time period of 2374.0 dimensionless time units is shown. Branch $1'$ bifurcates from branch 2 at $L \approx 56.7$ and ultimately corresponds to negative pulses at large L, as was found in Fig. 1(a). Two HB points on this branch at $L \approx 54.2$ and $L \approx 79.6$ produce time-periodic branches c and d which reconnect with the branch $1'$ each via a homoclinic bifurcation (these are shown with filled stars). Detail of the homoclinic snaking local to the homoclinic bifurcations corresponding to branches c and d can be seen in the insets in panel b. Consistent with the expected behaviour at a homoclinic bifurcation, we have checked that the time-period of the waves is $O(\log|L - L_c|)$ as $L \to L_c$, where L_c is the homoclinic bifurcation point (see, for example, 17, table 8.4.1). Note that the only stable part of branch $1'$ in the range shown is between the SN at $L \approx 53.9$ and the HB at $L \approx 54.2$. Branch $2'$ bifurcates from branch 2 and continues to large L, eventually producing a two-pulse bound state as was found in Fig. 1(a). It is unstable in the range shown. Branch $3'$ emerges from a PB at $L \approx 95.7$ and solutions on it are unstable up to the SN at $L \approx 95.2$ and is thereafter stable. At large L, solutions on branch $3'$ ultimately approach a two-pulse bound state which is distinct from the two-pulse bound state found on branch $2'$ at large L.

The diagrams imply that there exist L-windows of multistability. For example, branch 1 and branch 2 are both stable between $L \approx 66.5$ and $L \approx 78.3$.

4. Conclusions

We developed a novel numerical-continuation technique to obtain bound state solutions and to compute branches of time-periodic solutions in a travelling frame of reference for evolution equations with translational symmetry. We have applied the technique to the case of a long-wave model equation describing the motion of an electrified thin liquid film flowing down an inclined plane. In particular, we have constructed detailed

bifurcation diagrams illuminating the possible bound states and pulsating travelling waves. Construction of such bifurcation diagrams permits deeper insight into the dynamics of the system in question at particular parameter values. Finally, we note that branches stemming from Neimark–Sacker (torus) bifurcations (e.g. Kuznetsov [18]) cannot be followed using the present method and a new approach is required. This is left as a subject for future investigation.

Acknowledgements

We acknowledge financial support by the EPSRC under grants EP/J001740/1 and EP/K041134/1 and by the Ministry of Science and Technology of Taiwan under research grant MOST-103-2115-M-009-015-MY2.

Appendix A. Supplementary data

Supplementary material related to this article can be found online at https://doi.org/10.1016/j.aml.2018.06.034.

References

[1] T.-S. Lin, S. Rogers, D. Tseluiko, U. Thiele, Bifurcation analysis of the behaviour of partially wetting liquids on a rotating cylinder, Phys. Fluids 28 (2016) 082102.
[2] S.D. Zaidman, Topics in Pseudo-Differential Operators, Vol. 359, CRC Press, 1996.
[3] E.J. Doedel, H.B. Keller, J.P. Kernevez, Numerical analysis and control of bifurcation problems (I): Bifurcation in finite dimensions, Int. J. Bifurcation Chaos 1 (1991) 493–520.
[4] E.J. Doedel, B.E. Oldeman, AUTO07p: Continuation and bifurcation software for ordinary differential equations, Tech. rep. Concordia University 2012.
[5] M. Frigo, S.G. Johnson, The design and implementation of FFTW3, Proc. IEEE 93 (special issue on "Program Generation, Optimization, and Platform Adaptation") (2005) 216–231.
[6] G. Bordyugov, H. Engel, Continuation of spiral waves, Physica D 228 (2007) 49–58.
[7] A. Pototsky, U. Thiele, A. Archer, Coarsening modes of clusters of aggregating particles, Phys. Rev. E 89 (2014) 032144.
[8] H.S. Brown, I.G. Kevrekidis, A. Oron, P. Rosenau, Bifurcations and pattern formation in the "regularized" Kuramoto-Sivashinsky equation, Phys. Lett. A 163 (1992) 299–308.
[9] H. Uecker, U. Wetzel, J. Rademacher, pde2path–a Matlab package for continuation and bifurcation in 2D elliptic systems, Numer. Math. TMA 7 (2014) 58–106.
[10] H. Uecker, User guide on Hopf bifurcation and time periodic orbits with pde2path, Available at http://www.staff.uni-oldenburg.de/hannes.uecker/pde2path/tuts/hotut.pdf.
[11] J.D.M. Rademacher, H. Uecker, Symmetries, freezing, and Hopf bifurcations of traveling waves in pde2path, 2017. Available at http://www.staff.uni-oldenburg.de/hannes.uecker/pde2path/tuts/symtut.pdf.
[12] M.G. Blyth, D. Tseluiko, T.-S. Lin, S. Kalliadasis, Two-dimensional pulse dynamics and the formation of bound states on electrified falling films, submitted for publication. https://arxiv.org/abs/1706.04014.
[13] M. Pradas, D. Tseluiko, S. Kalliadasis, Rigorous coherent-structure theory for falling liquid films: Viscous dispersion effects on bound-state formation and self-organization, Phys. Fluids 23 (2011) 044104.
[14] I.G. Kevrekidis, B. Nicolaenko, J.C. Scovel, Back in the saddle again–a computer-assisted study of the Kuramoto-Sivashinsky equation, SIAM J. Appl. Math. 50 (1990) 760–790.
[15] U. Thiele, E. Knobloch, Thin liquid films on a slightly inclined heated plate, Physica D 190 (2004) 213–248.
[16] D. Tseluiko, M.G. Blyth, D.T. Papageorgiou, Stability of film flow over inclined topography based on a long-wave nonlinear model, J. Fluid Mech. 729 (2013) 638–671.
[17] S.H. Strogatz, Nonlinear Dynamics and Chaos, Westview Press, Boulder, 2014.
[18] Y.A. Kuznetsov, Elements of Applied Bifurcation Theory, Vol. 112, Springer Science & Business Media, 2013.